A Computational Investigation of NMR Properties of Mixed-Metal Niobate Perovskites

Rebecca Bisset
Supervised by Professor Sharon E. Ashbrook

University of
St Andrews

Introduction

Perovskites are a family of materials with the formula ABX_3 with wide-ranging properties and applications which have brought them much scientific interest. Niobate-based perovskites show promising electronic properties – such as ferroelectricity and piezoelectricity – leading to many applications from optical storage to sensors and actuators. Sodium niobate ($NaNbO_3$) derivatives – particularly $K_xNa_{1-x}NbO_3$ solid solutions – are very promising candidates to replace $Pb(Zr,Ti)O_3$ piezoelectrics, providing an effective yet non-toxic alternative.[1] The structure of perovskites is based upon an ideal of cubic symmetry of BX_6 octahedra and AX_{12} coordination, but this is often distorted by displacement of the A and B ions from their central positions.[2] Such distortions cause the properties of perovskites to be variable through substitution into these A- and B-sites. The structure of end-member $NaNbO_3$ at room temperature has been characterized to be formed primarily of the *Pbcm* and *P2₁ma* space group polymorphs, and $KNbO_3$ takes the space group *Amm2*.[3] In these polymorphs of $NaNbO_3$ there are two distinct A-sites – denoted A(1) and A(2) here, where 'A' may be Na or K – and the *Amm2* polymorph of $KNbO_3$ has just one A-site.

In mixed-metal compounds NMR analysis is favoured, as NMR spectroscopy is sensitive to an atomic-scale environment making it ideal for the structural characterisation of disordered materials. Despite the high oxygen content of niobate perovskites, the low natural abundance of the NMR-active isotope of oxygen, ^{17}O, of 0.038% means that costly oxygen-enrichment must be carried out on samples to yield interpretable results.[4] An alternative to this enrichment is the use of computation to simulate the NMR results of the different compositions of the solid solutions. In theory, this computation could provide a precursor to experimentation which allows later research to focus on the most-promising candidates.

This research utilizes density functional theory (DFT) which uses the total electron density and the positions of electrons to build an energy function – upon which calculations can run. DFT requires the use of functionals to model how electron density changes within infinitesimally small volume elements – generalised gradient approximations (GGAs) predict that this change is approximately linear in each volume element. The two functionals explored here, PBE and PBEsol, are both GGAs.[5,6]

When introducing substituted atoms into the end member structures, many different atomic configurations of the cations within the lattice is possible and so ensemble-based modelling is carried out using the Site Occupancy Disorder (SOD) program.[7] This minimises the number of distinct configurations of atoms, as many will be symmetry related and so can be taken to be equivalent, allowing the reduction of the sizes of the calculations.[7]

Method

The CASTEP code was used to carry out DFT calculations on the perovskite structures.[8] CASTEP uses gauge including projector augmented waves (GIPAWs),[8] and the generalised gradient approximations used were PBE and PBEsol.[5,6] The Brioullin space was sampled using a k-point spacing that was selected to be 0.04 $Å^{-1}$, and the cut-off energy for the planewaves used to approximate each wavefunction was set as 60 Ry. These values were chosen after checking the convergence of energy values for $NaNbO_3$ using a range of k-point spacings and cut-off energies. The end member crystal structures were obtained from the Inorganic Crystal Structure Database. The Site Occupancy Disorder program (SOD) was used to carry out ensemble-based modelling on the solid solution structures.[7] The end member structures (*Pbcm* and *P2₁ma* polymorphs of $NaNbO_3$, and $KNbO_3$) were optimised using both PBE and PBEsol functionals, and then NMR calculations carried out on each using both functionals again (generating four sets of NMR data) in order to investigate differences and advantages of the different functionals, before the PBE functional was selected to be used in both the optimisation and NMR calculations. The initial end member structures were of varying sizes – the *Pbcm* structure was Z=8, *P2₁ma* was Z=4 and *Amm2* was Z=2 – and so Z=8 supercells of each that were approximately 15 × 5 × 5 Å were generated and these analysed. Geometry optimisation was run on every structure

before NMR calculations. The NMR calculations yield values for the isotropic shielding, σ_{iso}, the magnitude of quadrupolar interaction, C_Q, and quadrupolar interaction asymmetry η_Q, and so for comparison to experimental results σ_{iso} must be converted to δ_{iso}:

$$\delta_{iso} = -(\sigma_{iso} - \sigma_{ref})$$

σ_{ref} is the reference isotropic shielding. σ_{ref} values were calculated using the ilmenite polymorph of $NaNbO_3$ and cristobalite (559.7 ppm for ^{23}Na and 261.5 ppm for ^{17}O, respectively). For $KNbO_3$ and both the *Pbcm* and *P2₁ma* polymorphs of $NaNbO_3$, a range of substitutions was produced by replacing sodium ion(s) with potassium ion(s) – $K_xNa_{1-x}NbO_3$ solid solutions were produced where x = 0, 0.125, 0.5, 0.875 and 1. SOD was used to find equivalent configurations of the x = 0.5 solid solutions.

Results and discussion

PBE *versus* PBEsol comparison

An initial investigation was carried out to compare the accuracy of the PBE and PBEsol functionals when used for optimisation and computational NMR analysis of sodium and potassium niobates. Comparisons were drawn between cell parameters, bond lengths and NMR parameters for the four resultant methods and experimental literature values.

Table 1: Comparison of bond lengths in the $NaNbO_3$ $P2_1ma$ polymorph using the PBE and PBEsol functionals.

Method	PBE	PBEsol	Literature[a,b]
Bond	Bond length (Å)	Bond length (Å)	Bond length (Å)
Nb-O	1.891	1.904	1.885
	1.893	1.903	1.894
	1.983	1.966	1.975
	1.986	1.97	1.979
	2.124	2.05	2.091
	2.128	2.058	2.101
Na(1)-O	2.322	2.31	2.465
	2.384	2.338	2.465
	2.384	2.338	2.526
	2.528	2.551	2.549
	2.68	2.68	2.734
	2.68	2.68	2.734
	2.682	2.711	2.871
	2.682	2.711	2.871
	3.137	3.092	3.009
	3.146	3.013	3.026
	3.338	3.248	3.061
	3.338	3.248	3.061
Na(2)-O	2.356	2.386	2.277
	2.369	2.387	2.301
	2.458	2.401	2.511
	2.458	2.401	2.511
	2.579	2.565	2.659
	2.579	2.565	2.659
	2.632	2.634	2.764
	2.632	2.634	2.764
	3.145	3.059	3.132

	3.331	3.206	3.132
	3.433	3.374	3.348
	3.433	3.374	3.369

[a] *Nb-O bond lengths from Johnston* et al..[10] [b] *Na-O bond lengths from Gouget* et al..[11]

The bond lengths given in table 1 are representative, on the most part, of the bond lengths for all three end members. On average, it was found that for *P2₁ma* the Na(1)-O bond lengths were 4.9% different to literature for PBE and 4.2% different for PBEsol. For the Na(2)-O bond lengths, this was 3.1% for PBE and 3.3% for PBEsol, and for Nb-O it was 0.7% for PBE and 1.1% for PBEsol. Similar results were observed for the *P2₁ma* polymorph of $NaNbO_3$ and for the $KNbO_3$ end members – although for *P2₁ma* PBEsol calculated the Nb-O bond lengths more accurately, as opposed to the Na(1)-O bonds, and for $KNbO_3$, all three sets of bond lengths were most accurately predicted by PBE.

Table 2 demonstrates that the PBE functional predicts a set of cell parameters for $KNbO_3$ which are closer to literature than PBEsol, and this was replicated in the cell parameters of the two $NaNbO_3$ polymorphs.

Upon use of the four methods (PBE-based optimisation with either PBE- or PBEsol-based NMR calculations, and PBEsol-based optimisation with either PBE- or PBEsol-based NMR calculations), each method performed fairly similarly – table 3 shows that for each parameter at each atomic site, a different method prevailed. Based upon the more accurate geometrical predictions of the PBE functional, paired with the longer computational times taken by the PBEsol-based calculations, it was determined that further results could be gathered using the PBE functional solely.

Relative Mixing Energies

Using the energy values CASTEP predicted for each structure, the relative mixing energies were calculated and plotted as a function of substitution. The computational values were compared to theoretical energy values for the substituted structures calculated from the CASTEP energies of the end members. For example, the theoretical energy of $K_{0.125}Na_{0.875}NbO_3$ for a given polymorph would be:

$$E_{theoretical} = \left(0.125 \times E_{computational}^{KNbO_3}\right) + (0.875 \times E_{computational}^{NaNbO_3})$$

The relative mixing energies are then found by calculating the difference between $E_{theoretical}$ and $E_{computational}$.

*Table 2: Comparison of the $KNbO_3$ (*Amm2 *polymorph) cell parameters to experimental literature.*

Cell parameter	PBE	PBEsol	Literature value[9]	PBE % difference to literature	PBEsol % difference to literature
a (Å)	3.9564	3.9412	3.971	0.368	0.753
b (Å)	5.6637	5.6164	5.697	0.586	1.425
c (Å)	5.6866	5.6282	5.723	0.638	1.670

*Table 3: Comparison of the NMR parameters for the NaNbO3 (*Pbcm *polymorph) using the four methods.*

Species	Isotropic shift (ppm)					C_Q (MHz)					Quadrupolar asymmetry η_Q				
	PBE opt.		PBEsol opt.		Literature	PBE opt.		PBEsol opt.		Literature	PBE opt.		PBEsol opt.		Literature
	PBE NMR	PBEsol NMR	PBE NMR	PBEsol NMR		PBE NMR	PBEsol NMR	PBE NMR	PBEsol NMR		PBE NMR	PBEsol NMR	PBE NMR	PBEsol NMR	
Na(1)	-1.02	-1.09	-1.35	-1.42	-0.5(5) [11]	3.25	3.07	3.18	3.01	2.1(1) [11]	0.17	0.18	0.18	0.19	0.0(1) [11]
Na(2)	-6.38	-6.46	-5.71	-5.75	-4.2(5) [11]	-1.10	-1.03	1.20	1.13	1.0(2) [11]	0.54	0.56	0.86	0.83	0.8(1) [11]
Nb	-	-	-	-	-	21.6	21.4	-14.4	-14.5	19.5 (7) [12]	0.77	0.8	0.77	0.75	0.7(1) [12]

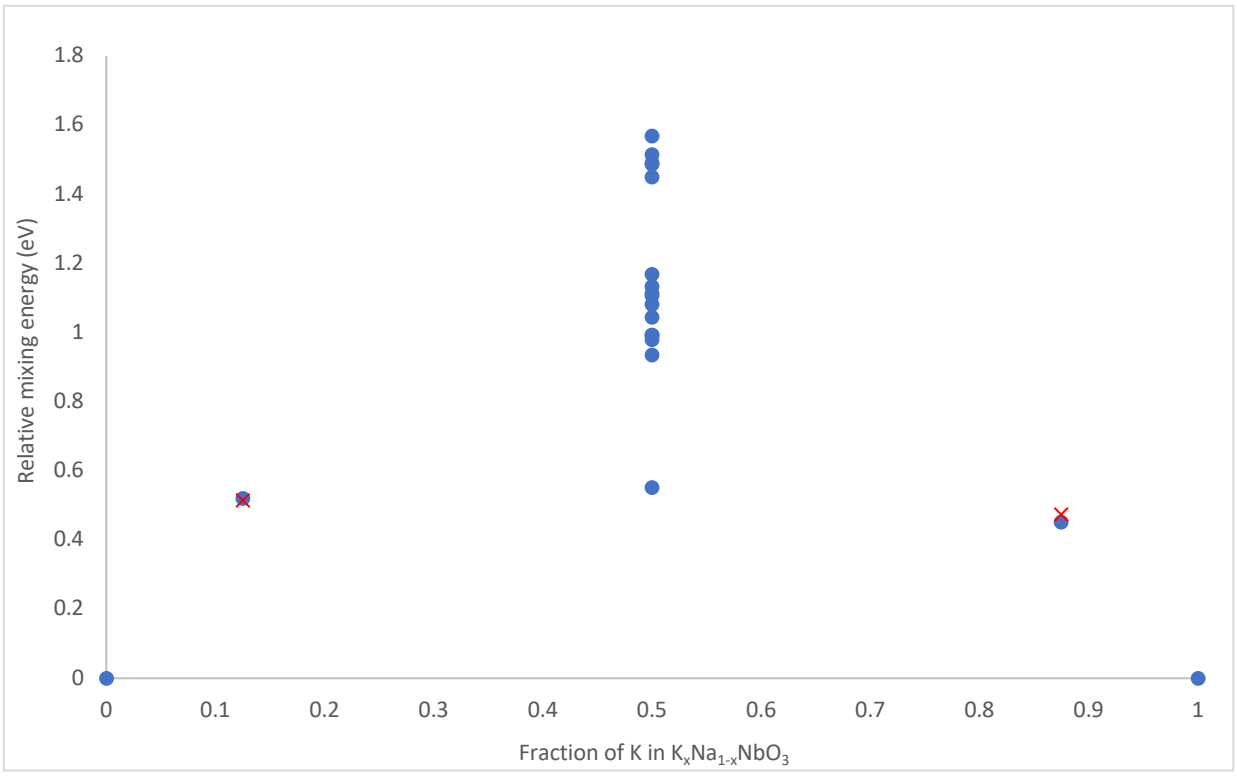

Figure 1: Pbcm-*based relative mixing energies plotted as a function of the fraction of K in* $K_xNa_{1-x}NbO_3$*. The red cross markers denote the configurations where the substitution has been made in a A(1)-site – for x = 0.125 this is one K ion in an A(1)-site, and for x = 0.875 this is one Na ion in a A(1)-site.*

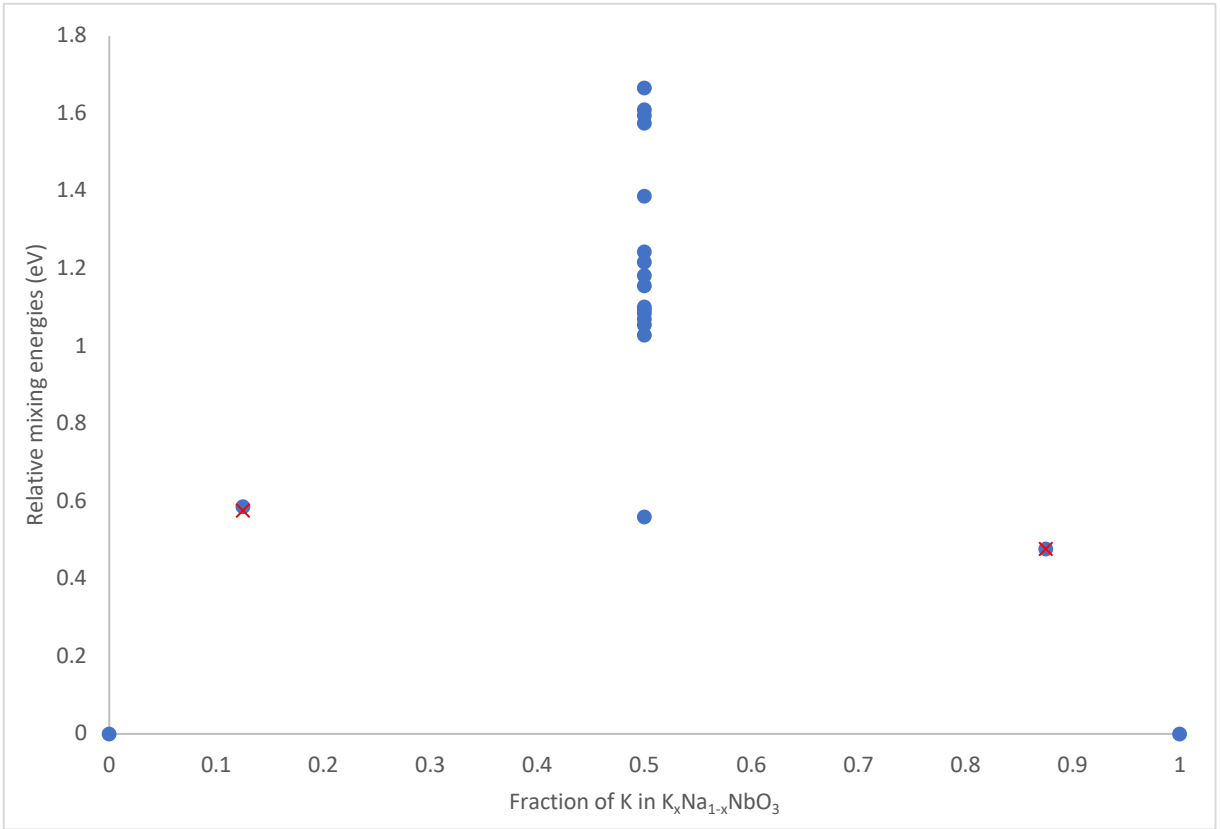

Figure 2: $P2_1ma$-*based relative mixing energies plotted as a function of the fraction of K in* $K_xNa_{1-x}NbO_3$*. The red cross markers denote the configurations where the substitution has been made in a "(1)" site – for x = 0.125 this is one K ion in an Na(1) site, and for x = 0.875 this is one Na ion in a "K1" site.*

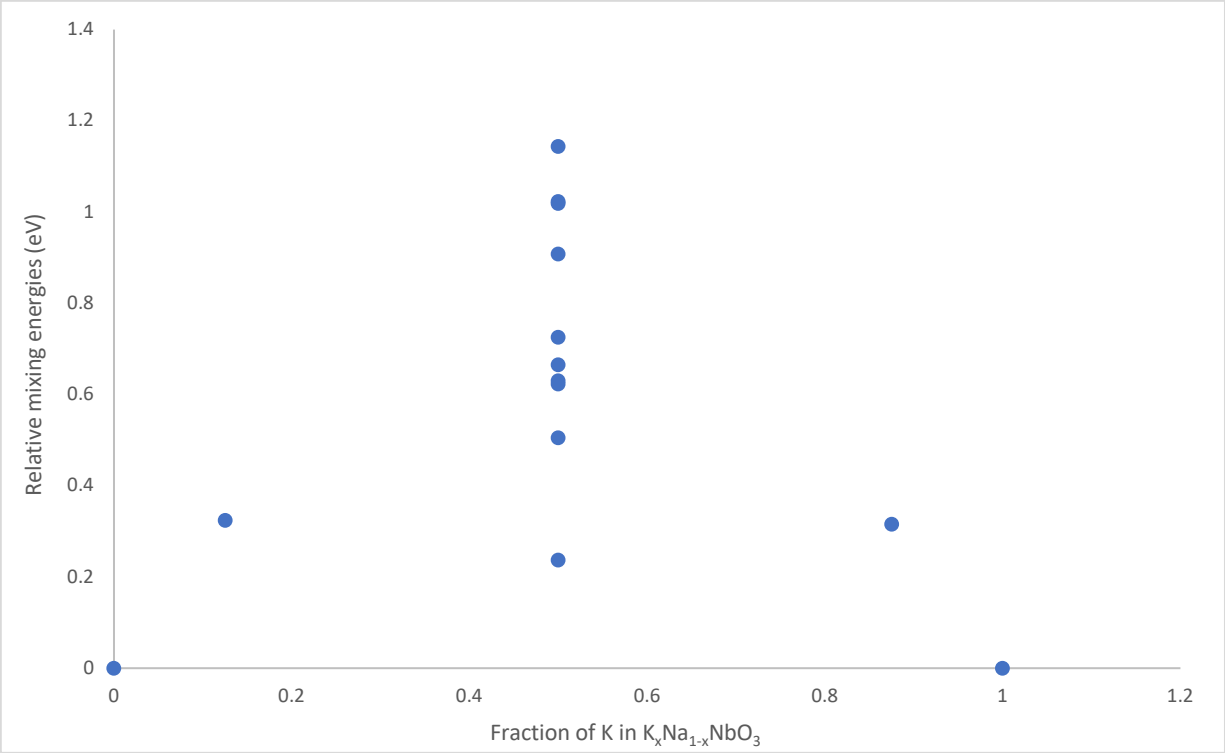

Figure 3: Amm2*-based relative mixing energies plotted as a function of the fraction of K in* $K_xNa_{1-x}NbO_3$.

For all three sets of substitutions, the energy values as determined by CASTEP are more positive than the theoretical energy values calculated. This indicates that the substitutions of K into a $NaNbO_3$ structure and of Na into a $KNbO_3$ structure are more disfavoured than the end members predict. This is also indicated by examination of the highest and lowest energy configurations of the x = 0.5 structures.

Figure 4 shows the highest and lowest energy configurations of the *Amm2*-based polymorph of $K_{0.5}Na_{0.5}NbO_3$. These structures also suggest the slight unfavorability of the mixing of K and Na ions within these perovskite structures – the highest energy configuration has the largest degree of mixing between the ions, whereas the lowest energy configuration has a clear separation of Na-based regions and K-based regions. Also of note is the distinction in energy values depending on whether substitution has occurred in the A(1)- or A(2)-site. In both *Pbcm* and *P2₁ma* sets, the presence of a single K ion in an Na(1) site was favourable to a substitution in an Na(2) site. Similarly, substitution of a single Na into a "K(2)" site is preferential to substituting a Na ion into a "K(1)" site. The descriptions of "K(1)" and "K(2)" are used to distinguish that this is a sodium ion being substituted back into a theoretical $KNbO_3$ end member based on the *Pbcm/P2₁ma* $NaNbO_3$ end members - taking the structure from x = 1 to x = 0.875.

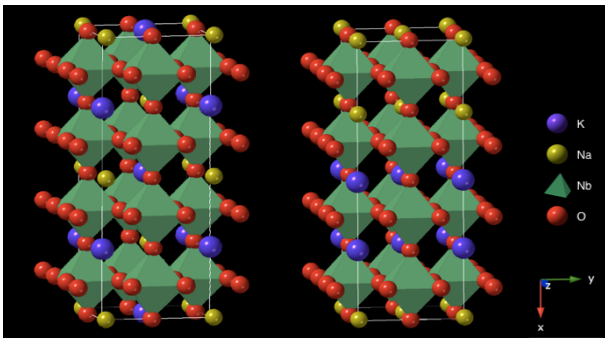

Figure 4: Highest (left) and lowest (right) energy configurations of the $K_{0.5}Na_{0.5}NbO_3$ (Amm2 *polymorph) using CrystalMaker®.*[11]

<u>NaO Bond Lengths</u>

$NaNbO_3$ would have NaO_{12} coordination in an ideal perovskite. The bond length of Na-O in these perovskite structures can be predicted to be 2.79 Å, using the ionic radii of Na^+ and O^{2-}.[13] The twelve shortest Na-O distances were compiled for each Na species in each configuration and the results are

given in figures 5-7. Note that for $K_{0.5}Na_{0.5}NbO_3$ only the highest and lowest energy configurations are presented.

The Na-O bond lengths observed in the three polymorphs differ in trends. The *Pbcm*- and *P2₁ma*-based substitution sets appear to have two 'bands' of bond lengths, most clearly defined at the Na end member. For both polymorphs, as the fraction of K increases, the two bands start to merge and the range of results narrows. The presence of these two clear bands, separated by ~0.3-4 Å at the $NaNbO_3$ end member in both cases, could be indicative of the outer reaches of the NaO coordination. It can be observed that where the fraction of K present in the *Pbcm*- and *P2₁ma*-based sets is low, the lower band of Na-O distances has an upper limit of ~2.8 Å – which corresponds with the predicted bond length of 2.79 Å. There are seven distinct bond lengths noted in the upper band of the *Pbcm* Na end member, and eight in the *P2₁ma* Na end member. Each of these is four-times degenerate within the Z=8 supercells used. Using *CrystalMaker®* to visualise the structures,[12] it was found that three of the longer distances were associated with the Na(1) site of *Pbcm* $NaNbO_3$ and four were associated with Na(2) of *Pbcm* $NaNbO_3$ and both Na(1) and Na(2) of *P2₁ma* $NaNbO_3$. This would in turn result in coordinations of NaO_9 and NaO_8, respectively, as opposed to the ideal NaO_{12}.

All three of the Na end members also have less variation in bond lengths than the structures containing K. This is most noticeable in the *Amm2*-based set, where all eight Na species (each with twelve Na-O distances) give rise to five narrow groups of Na-O distances. The *Amm2*-based set also appears to lack the clear two-band division due to the defined groups of bond distances, although the results can be seen to again narrow slightly towards a Na-O distance of ~2.85 Å. If the same strategy as above is applied to the *Amm2* $NaNbO_3$ end member, there are 2 bond lengths above the 3 Å point – of degeneracies that would give rise to a NaO_7 coordination.

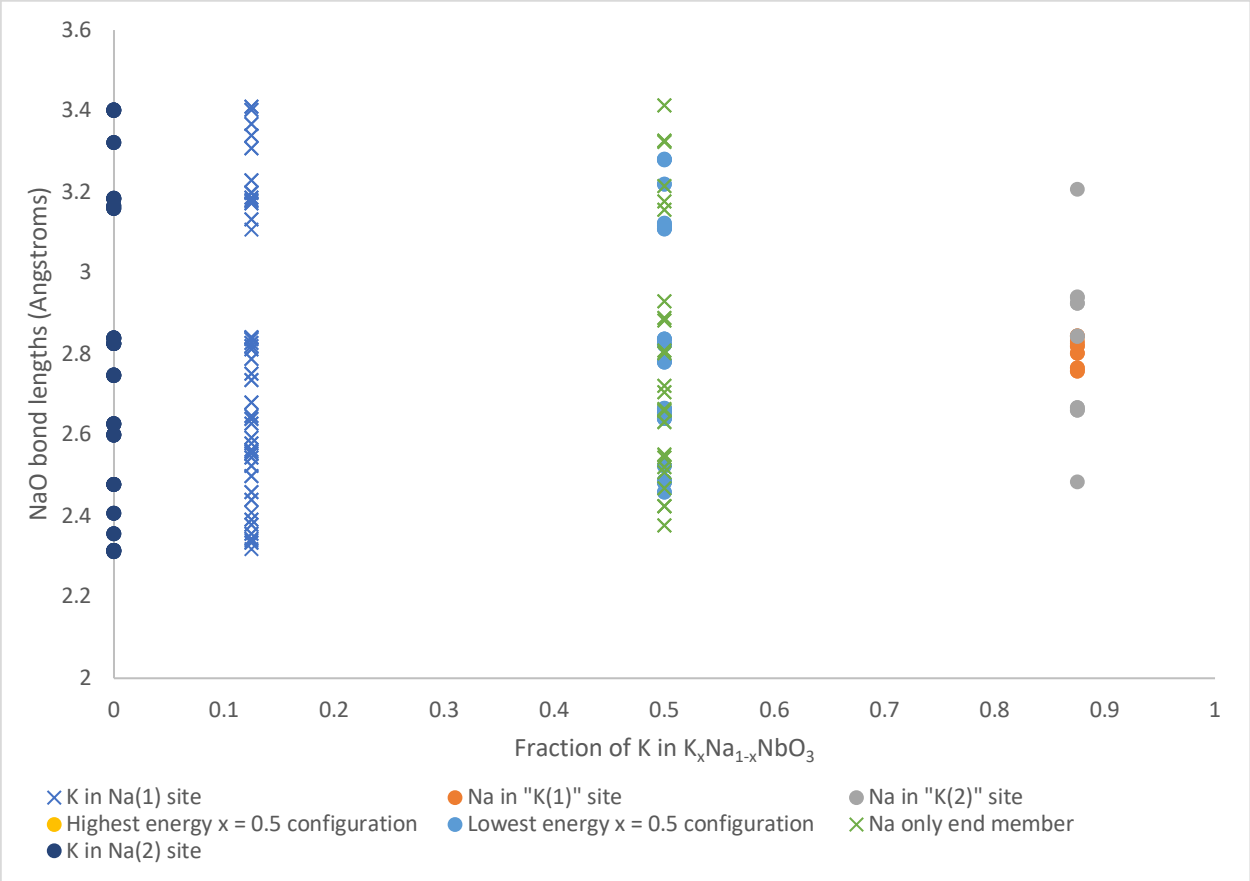

Figure 5: NaO bond lengths as a function of K fraction in $K_xNa_{1-x}NbO_3$ (using Pbcm *polymorph)*

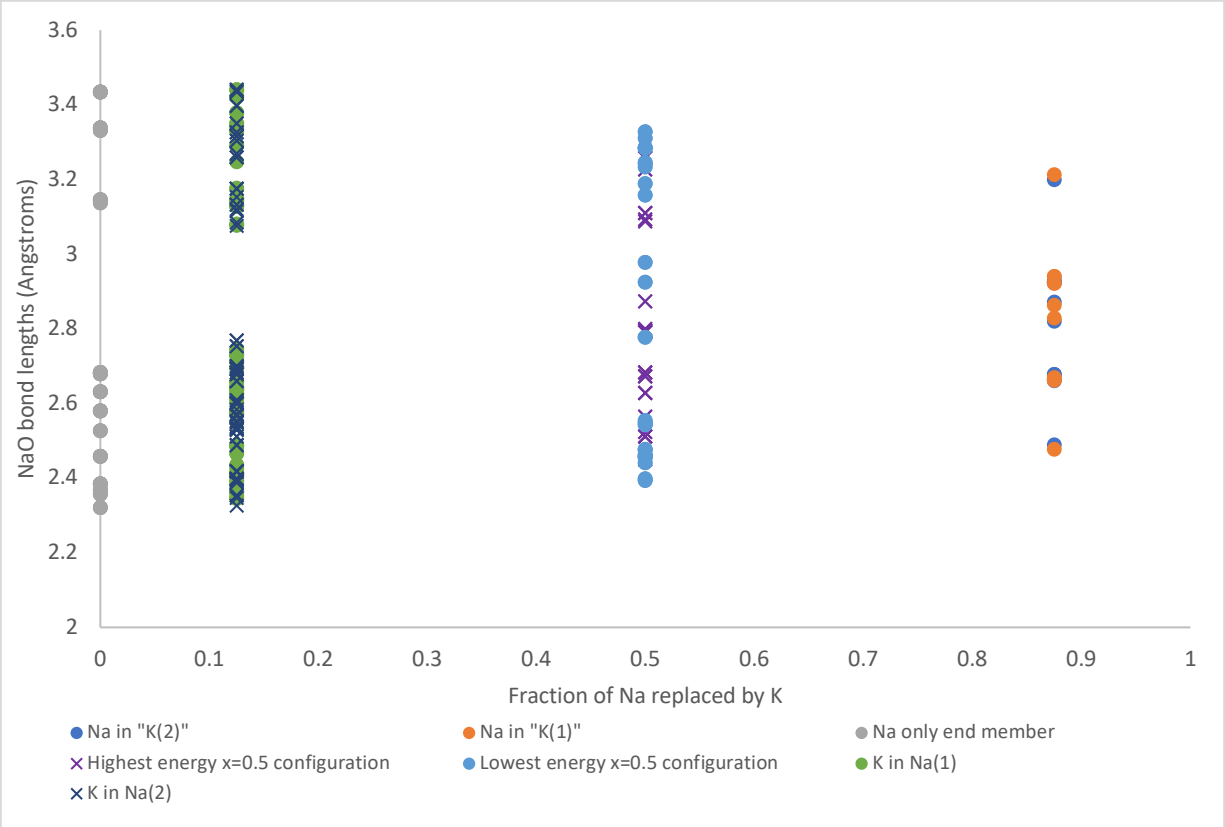

Figure 6: NaO bond lengths as a function of K fraction in $K_xNa_{1-x}NbO_3$ (using $P2_1ma$ polymorph)

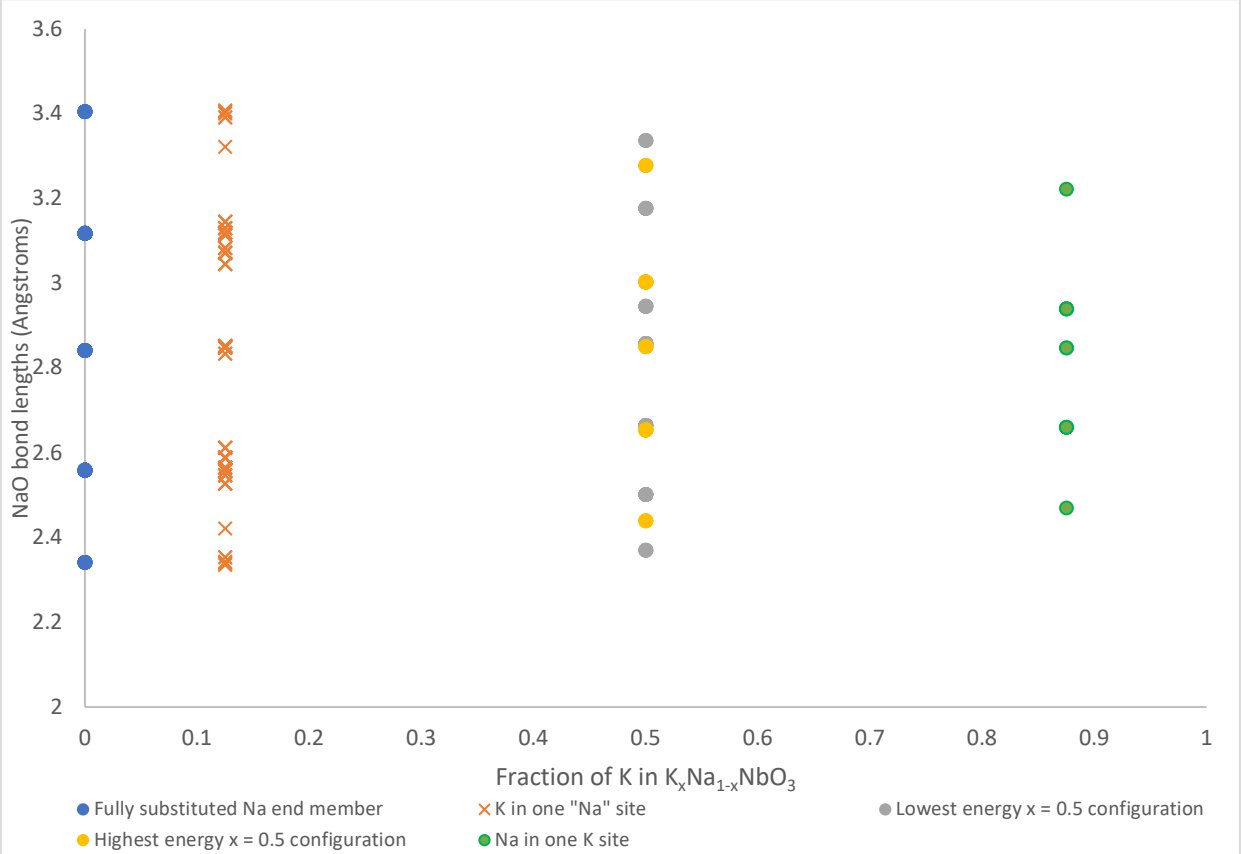

Figure 7: NaO bond lengths as a function of K fraction in $K_xNa_{1-x}NbO_3$ (using Amm2 polymorph)

Table 4: ^{23}Na NMR results using CASTEP for the Pbcm-, $P2_1ma$- *and* Amm2*-based sets.*

Initial polymorph of end member			***Pbcm***			***$P2_1ma$***			***Amm2***		
Structure description	Fraction of K	Site	δ_{iso} (ppm)	C_Q (MHz)	η_Q	δ_{iso} (ppm)	C_Q (MHz)	η_Q	δ_{iso} (ppm)	C_Q (MHz)	η_Q
$NaNbO_3$ end member	0	Na1	-1.0 [-0.5(5)]	3.25 [2.1(1)]	0.17 [0.0(1)]	1.5 [-1.4(5)]	-1.49 [2.1(1)]	0.82 [0.9(1)]	-16.4	0.84	0.81
		Na2	-6.4 [-4.2(5)]	-1.1 [1.0(2)]	0.54 [0.8(1)]	-4.1 [-5.1(5)]	-1.02 [1.1(2)]	0.32 [0.7(1)]	-	-	-
K in one A1 site	0.125	Na1	-2.1	3.11	0.10	-6.8	-1.03	0.37	-16.2	0.87	0.57
		Na2	-3.2	2.90	0.17	-7.0	-0.69	0.45	-16.9	0.89	0.66
		Na3	-8.2	2.36	0.35	-7.0	0.68	0.47	-17.0	0.78	0.88
		Na4	-8.9	-1.10	0.49	0.2	-1.61	0.82	-16.8	0.85	0.91
		Na5	-8.8	-0.85	0.69	-5.5	1.59	0.95	-20.3	0.62	0.98
		Na6	-	-	-	-0.7	1.47	0.99	-	-	-
K in one A2 site	0.125	Na1	-5.4	2.65	0.10	-6.0	-0.92	0.28	-	-	-
		Na2	-4.4	2.65	0.16	-5.1	-1.06	0.37	-	-	-
		Na3	-8.4	-0.92	0.62	-8.1	-1.16	0.61	-	-	-
		Na4	-10.6	-1.15	0.65	-2.0	1.38	0.85	-	-	-
		Na5	-7.1	-1.26	0.67	-2.0	-1.57	0.88	-	-	-
Intermediate E config.	0.5	Na1	-13.4	1.37	0.02	-13.7	0.43	0.1	-19.6	0.71	0.49
		Na2	-13.3	1.36	0.03	-	-	-	-	-	-
Lowest E config.	0.5	Na1	-9.5	1.83	0.28	-10.1	-0.91	0.49	-16.5	0.76	0.66
		Na2	-11.0	-1.26	0.77	-5.4	0.97	0.63	-	-	-
Highest E config.	0.5	Na1	-14.1	1.48	0.28	-15.9	1.42	0.50	-21.9	0.60	0.06
		Na2	-15.5	0.66	0.70	-16.1	0.80	0.83	-	-	-
Na in one A1 site	0.875	Na1	-22.0	-0.46	0.20	-20.7	0.57	0.45	-20.7	0.60	0.43
Na in one A2 site	0.875	Na1	-20.3	0.57	0.51	-21.0	0.56	0.50	-	-	-

Note that the 'fraction of K' is the fraction of potassium in the $K_xNa_{1-x}NbO_3$ solid solution. Also, the configurations for x = 0.5 given are the highest, lowest and (one) intermediate energy configurations for each polymorph. The values in square brackets [] are from experimental literature.[14] Note that experimentally, only the absolute value of C_Q can be determined, whereas the computational C_Q values can be positive or negative.

NMR Properties

The calculations run by CASTEP predicted results for ^{17}O, ^{23}Na, ^{39}K and ^{93}Nb NMR analysis done on each structure. This research will mainly focus on ^{17}O and ^{23}Na NMR – to limit need to carry out ^{17}O NMR experimentally unnecessarily, and because ^{23}Na NMR can yield key information about potassium present in structures whilst being easily reproducible experimentally. ^{39}K NMR is difficult to carry out due it being a low-γ nucleus.

Table 4 gives the ^{23}Na NMR results predicted by CASTEP for the range of substitutions, based on each polymorph, as well as literature values for the *Pbcm* and *P2₁ma* $NaNbO_3$ end members. A few of the computational values are slightly out with the experimental range of values given by literature.[3] For the isotropic shift values, small discrepancies may be down to the calculation of σ_{ref}. The computational and experimental results do however show similar trends between the three parameters related to each sodium site.

Upon compiling the ^{23}Na NMR results, a trend was immediately apparent – as the fraction of K in the solid solution increases, the isotropic shifts of Na species decrease. Figures 8-10 show the trend in the three sets of results. It is a strong correlation in the *Pbcm* and *P2₁ma* sets, and a weaker one in the *Amm2* set. The range of isotropic shifts decreasing means the shielding of the Na species increase as the fraction of K present increases – potassium is a larger and more electropositive species than sodium and so its introduction provides more electron shielding for remaining sodium atoms.

Figures 11-13 show the relationship between the isotropic shifts of the ^{17}O species and C_Q, for the range of substitutions. Note that only three configurations for the $x = 0.5$ sets are shown in each figure to reduce overcrowding, but all showed similar values. For ^{17}O, a higher fraction of K can be seen to cause a gradual increase in the isotropic shifts.

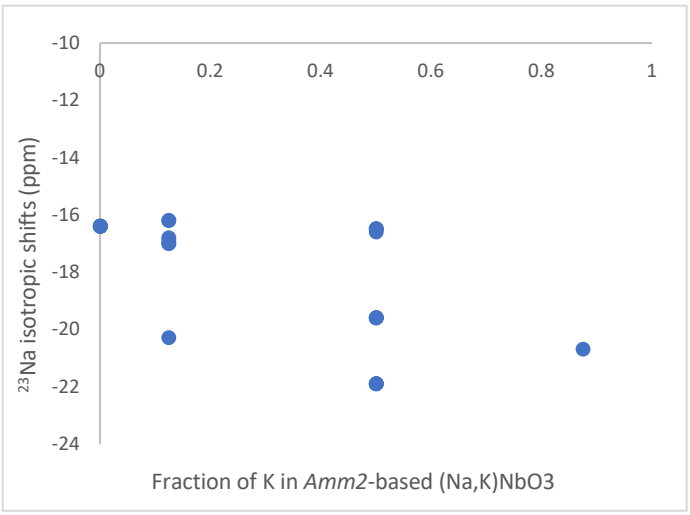

Figure 8: Variation of ^{23}Na isotropic shifts predicted by CASTEP as a function of K in Amm2*-based $K_xNa_{1-x}NbO_3$.*

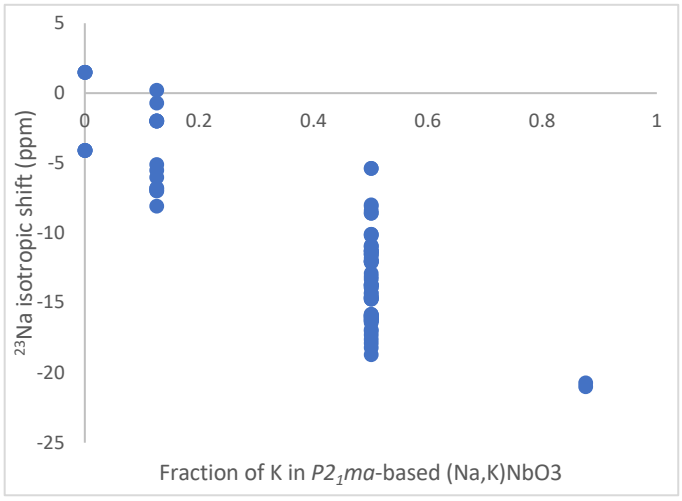

Figure 9: Variation of ^{23}Na isotropic shifts predicted by CASTEP as a function of K in P2₁ma*-based $K_xNa_{1-x}NbO_3$.*

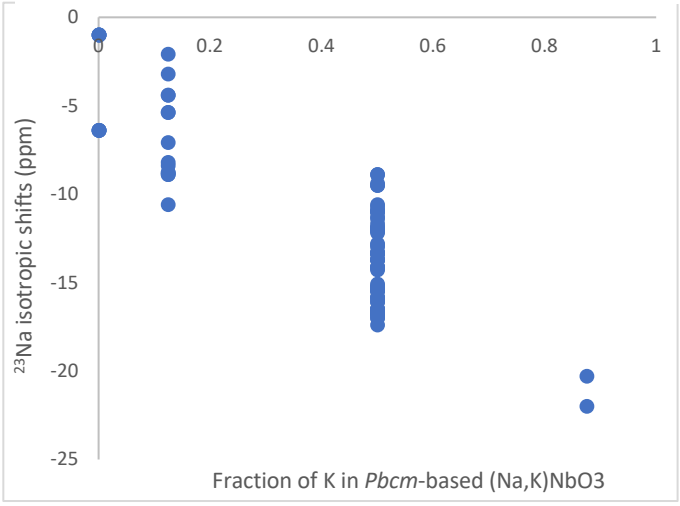

Figure 10: Variation of ^{23}Na isotropic shifts predicted by CASTEP as a function of K in Pbcm*-based $K_xNa_{1-x}NbO_3$.*

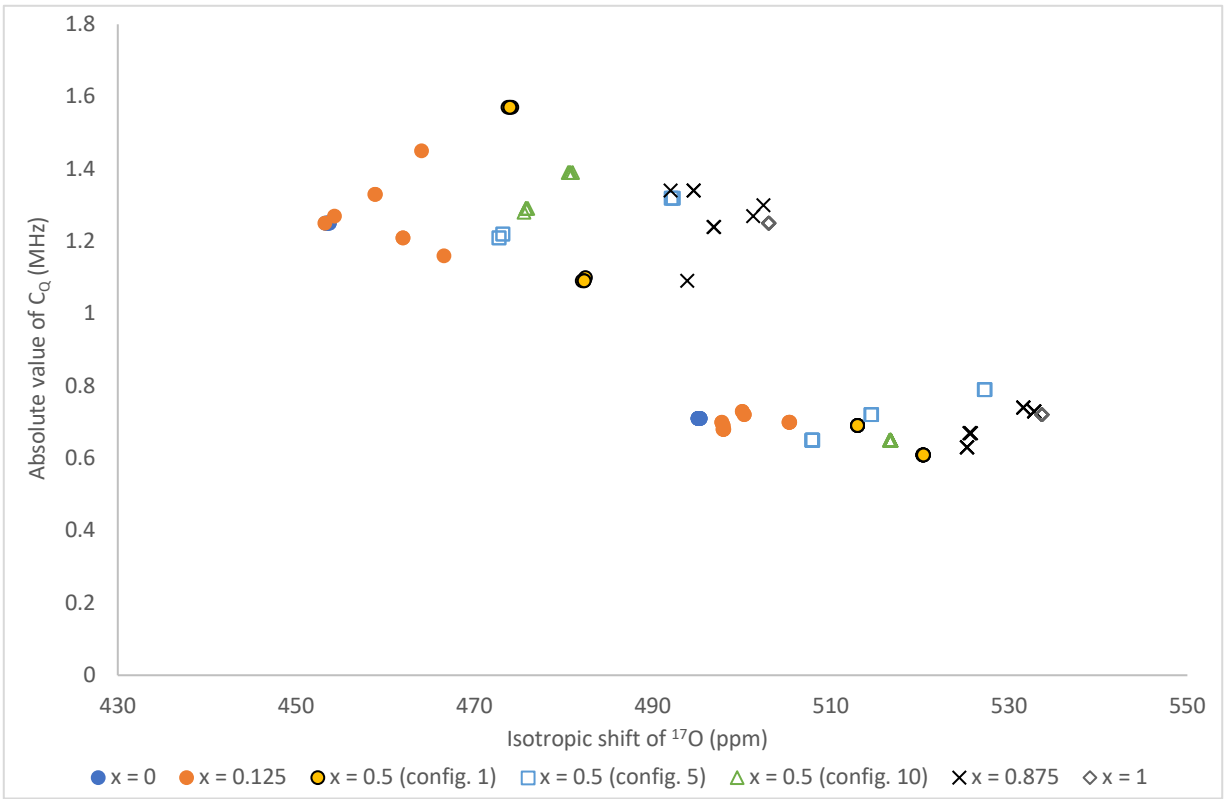

Figure 11: Amm2*-based results for ^{17}O NMR using CASTEP shown as the relationship between the isotropic shift and C_Q for the range of substitutions. Note that configurations 5 and 10 relate to the lowest and highest energy configurations of the x = 0.5 set, respectively, and config. 1 is of an intermediate energy.*

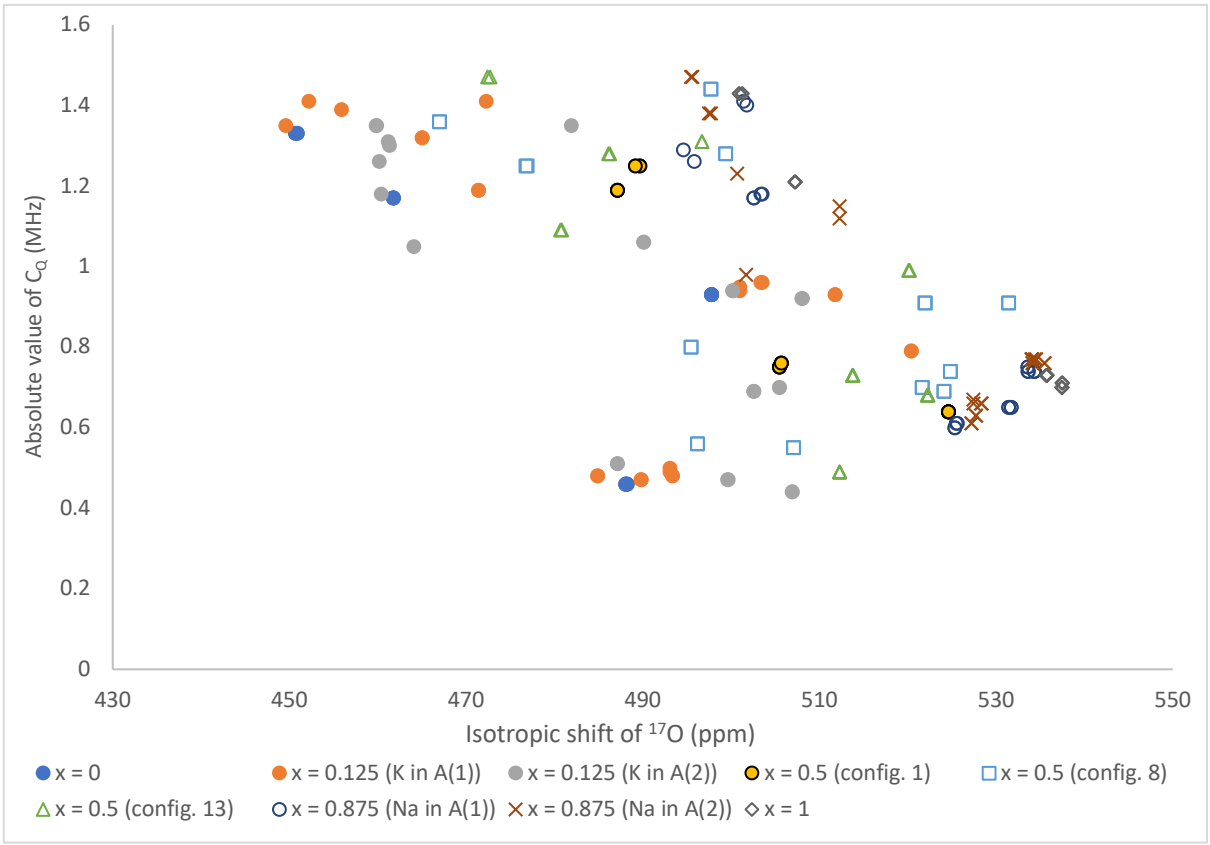

Figure 12: Pbcm*-based results for ^{17}O NMR using CASTEP shown as the relationship between the isotropic shift and C_Q for the range of substitutions. Note that configurations 8 and 13 relate to the lowest and highest energy configurations of the x = 0.5 set, respectively, and config. 1 is of an intermediate energy.*

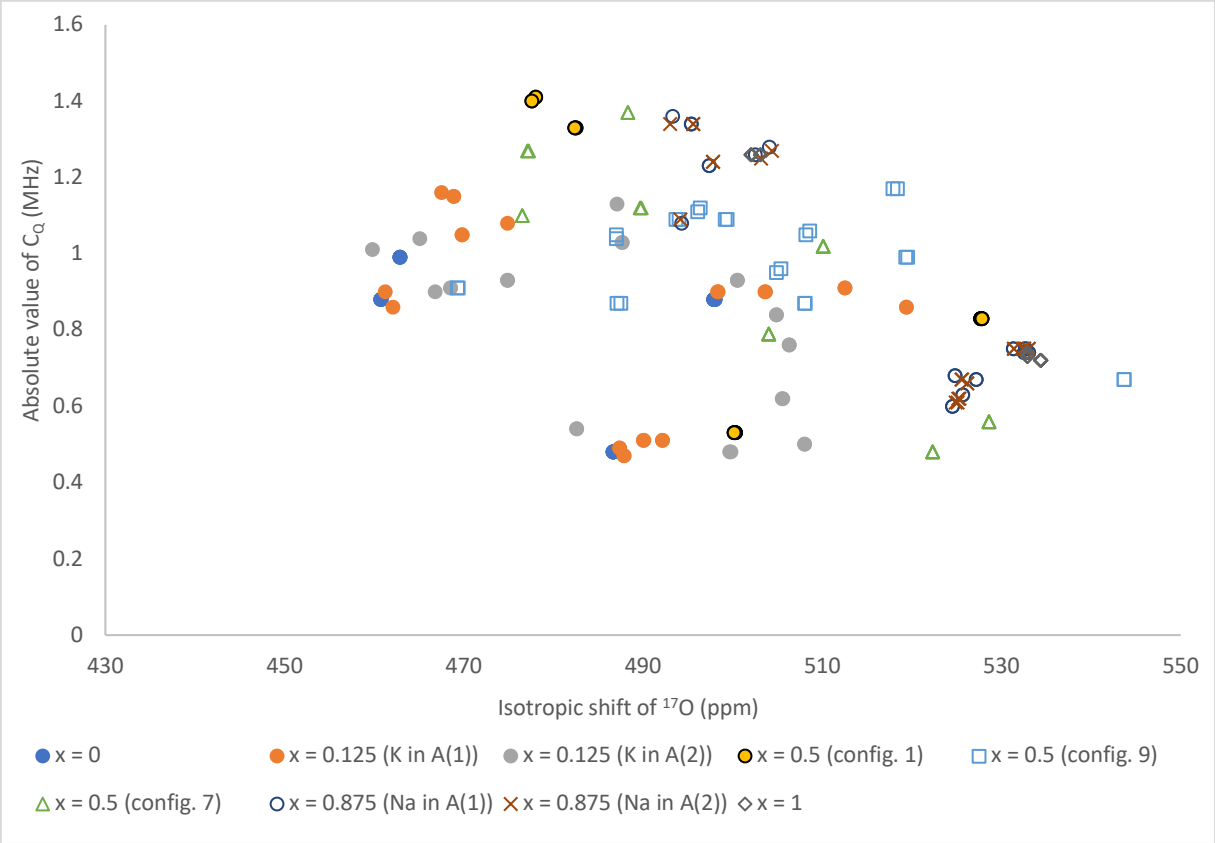

Figure 13: $P2_1ma$*-based results for* ^{17}O *NMR using CASTEP shown as the relationship between the isotropic shift and* C_Q *for the range of substitutions. Note that configurations 9 and 7 relate to the lowest and highest energy configurations of the x = 0.5 set, respectively, and config. 1 is of an intermediate energy.*

Conclusion

A range of $K_xNa_{1-x}NbO_3$ solid solutions were successfully simulated using *Pbcm* and *P2₁ma* polymorphs of $NaNbO_3$ and $KNbO_3$ as the initial end members. These were used to compare the DFT functionals of PBE and PBEsol for the purpose of geometry optimisation and predicting NMR parameters of the solid solutions, to find that PBE was an acceptable choice for this research. From there, the solid solutions were each analysed to find that the relative mixing energies were positive for all three polymorph sets, meaning the formation of mixed-metal niobate structures is slightly disfavoured relative to the end members. The NaO bond lengths were compiled as a function of the K content of the solid solution and compared to the bond length predicted by use of ionic radii. The ^{23}Na and ^{17}O NMR parameters of δ_{iso}, C_Q and η_Q were gathered and the relationship between increasing K fraction in the solid solution was linked to a decrease in isotropic shift for ^{23}Na, and increase in isotropic shift for ^{17}O.

Future Work

There is a lot of opportunity for future work related to this research. Further computational research could be done using slightly different solid solution compositions (*i.e.* using larger supercells to achieve finer increments of substitutions), or to investigate the similar compound $LiNbO_3$, and related solid solutions, which has also been found to be of interest in electronic applications.[14] Experimental work could also be done in synthesising structures of promise and comparing the results to those computationally found here.

Acknowledgements

I would like to thank my supervisor, Professor Sharon Ashbrook, for all the help and support she provided during this project, as well as the whole Ashbrook group – particularly Zachary Davis, Ben Griffiths and Emma Borthwick. I must give a huge thank you to Lord Laidlaw of Rothiemay, and the Laidlaw Foundation, whose funding made this project possible.

References

1 G. F. Teixeira, E. S. Junior, A. Z. Simões, E. Longo, M. A. Zaghete, *CrystEngComm.*, 2017, **19**, 4378-4392.

2 P. M. Woodward, *Acta Crystallogr., Sect. B: Struct. Sci.,* 1997, **53**, 32-44.

3 K. E. Johnston, C. C. Tang, J. E. Parker, K. S. Knight, P. Lightfoot, S. E. Ashbrook, *J. Am. Chem. Soc.,* 2010, **132**, 8732-8746.

4 D. Jardón-Álvarez, G. Reuveni, A. Hardchol, M. Leskes, *J. Phys. Chem. Lett.*, 2020, **11**, 5439-5445.

5 J. P. Perdew, K. Burke, M. Ernzerhof, *Phys. Rev. Lett.*, 1996, **77**, 3865-3868.

6 J. P. Perdew, A. Ruzsinszky, G. I. Csonka, O. A. Vydrov, G. E. Scuseria, L. A. Constantin, X. Zhou, K. Burke, *Phys. Rev. Lett.*, 2008, **100**, DOI: 10.1103/PhysRevLett.100.136406

7 R. Grau-Crespo, S. Hamad, C. R. A. Catlow, N. H. de Leeuw, *J. Phys. Condens. Matter*, 2007, **19**, DOI: 10.1088/0953-8984/19/25/256201.

8 S. J. Clark, M. D. Segall, C. J. Pickard, P. J. Hasnip, M. I. J. Probert, K. Refson, M. C. Payne, *Z. Kristallogr.*, 2005, **220**, 567-570.

9 L. Katz and H. D. Megaw, Acta. Cryst., 1967, **22**, 639-648

10 K. E. Johnston, J. M. Griffin, R. I. Walton, D. M. Dawson, P. Lightfoot, S. E. Ashbrook, *Phys. Chem. Chem. Phys.,* 2011, **13**, 7565-7576.

11 G. Gouget, M. Duttine, E. Durand, A. Villesuzanne, V. Rodriguez, F. Adamietz, T. Le Mercier, M. Braida, A. Demourgues, *ACS Appl. Electron. Mater.*, 2019, **1**, 513-522.

12 D. C. Palmer, S. E. Palmer, *CrystalMaker* (version 10.6.0), CrystalMaker Software Ltd, Begbroke, Oxfordshire, England, 2020.

13 R. D. Shannon, *Acta Cryst.*, 1976, **A32**, 751-767.

14 M.D Peel, S. E. Ashbrook, P. Lightfoot, *Inorg. Chem.,* 2013, **52**, 8872-8880.